Analytical Methods

PAPER

View Article Online
View Journal | View Issue

Cite this: *Anal. Methods*, 2017, **9**, 6061

Microprofiling real time nitric oxide flux for field studies using a stratified nanohybrid carbon–metal electrode†

P. Chaturvedi,[a] D. C. Vanegas,[b] B. A. Hauser,[c] J. S. Foster,[d] M. S. Sepúlveda[e] and E. S. McLamore *[a]

Nitric oxide (NO) is an important signaling molecule that is involved in stress response, homeostasis, host defense, and cell development. In most cells, NO levels are in the femtomolar to micromolar range, with extracellular concentrations being much lower. Thus, real time measurement of spatiotemporal NO dynamics near the surface of living cells/tissues is a major challenge. Here, we report the development, application, and validation of a self referencing (*i.e.*, oscillating) NO microelectrode for field studies of biological cells and tissues. The durable microelectrode is based on a hybrid nanomaterial composed of nanoceria, reduced graphene oxide and nanoplatinum and is intended for field use. One of the main focuses was to address the common pitfall of high overpotential through use of hydrophobic, and size/charge-selective materials in a thin film coated on top of the nanocatalyst sensor. The sensitivity (0.95 ± 0.03 pA nM^{-1}), response time (1.1 ± 0.1 s), operating potential (+720 mV), and selectivity of the nanomaterial-modified microelectrode are similar to laboratory microelectrode designs, enabling studies of NO flux in field studies. NO efflux was first measured from chitosan and alginate polymers in abiotic studies, and a deterministic model used to determine the effective diffusion coefficient for each polymer composite. To demonstrate the practicality of the sensor, NO flux was quantified in three model organisms with known NO pathways, including: bacteria, plant, and an invertebrate animal. For each organism, an established hypothesis was validated based on NO flux measurement and the results confirm data collected using standard analytical techniques. The sensor can be used to expand our fundamental knowledge of NO transport by facilitating field experiments which are not possible with standard techniques.

Received 14th August 2017
Accepted 11th October 2017

DOI: 10.1039/c7ay01964e

rsc.li/methods

Introduction

Oxygen and nitrogen radicals, such as superoxide anion (O_2^-), hydrogen peroxide (H_2O_2), and nitric oxide (NO) are chemically reactive cellular byproducts that form as a result of metabolic reactions in response to various stimuli. Radicals are important signaling molecules and regulate complex cellular functions, such as stress response and development. In most cells, radicals have a half-life of 0.5 to 5 s (with the exception of superoxide), although this can be prolonged when there are organics and/or biomolecules present in solution.[1] NO exists in three interconvertible forms: NO radical, NO^+ nitrosonium cation, and nitroxyl radical NO^-. *In vivo* concentration of NO is within the femtomolar to micromolar range in most cells.[2] In animals including invertebrates, NO is a key signaling molecule involved in a number of processes such as homeostasis, host defense, and development.[3–5] In plants, NO signaling has been linked to germination, growth rate of pollen tubes, stomatal movement, programmed cell death, and as a signaling and disease resistant molecule under stress conditions.[6–9] In bacteria, NO plays a unique role in toxin biosynthesis, regulation of recovery from radiation damage, nitration of different metabolites, and plant pathogenicity.[10,11] The high chemical reactivity, spatio-temporal variability, and diverse signaling role of NO, together with the low concentration in solution make its measurement in physiological conditions very challenging. This is particularly true for individual cells and small organisms.

As reviewed by a number of authors, there is a wide range of technologies for monitoring NO.[12–14] Examples include spectroscopic methods (*e.g.*, chemiluminescence and UV-visible spectroscopy), indirect methods (*e.g.*, colorimetric assays,

[a]*Agricultural and Biological Engineering Department, Institute of Food and Agricultural Sciences, University of Florida, Gainesville, FL, USA. E-mail: emclamor@ufl.edu*

[b]*Food Engineering Department, Universidad del Valle, Cali, Colombia*

[c]*Department of Biology, University of Florida, Gainesville, FL, USA*

[d]*Department of Microbiology and Cell Sciences, University of Florida, Space Life Science Lab, Merritt Island, FL, USA*

[e]*Department of Forestry and Natural Resources, Purdue University, West Lafayette, IN, USA*

† Electronic supplementary information (ESI) available. See DOI: 10.1039/c7ay01964e

capillary electrophoresis), fluorescent probes, spin trap electroparamagnetic resonance spectroscopy, and electrochemical electrodes. To be useful for measuring NO in living systems, technologies must: (i) have quantitative sensitivity, (ii) be highly selective, (iii) have a rapid response time, (iv) be capable of detecting NO in the nM range, (v) have little or no signal hysteresis, and (vi) be non-invasive (*i.e.*, label free and non-contact). As discussed in the review by Zhang *et al.*[2] many of the aforementioned techniques lack the required quantitative sensitivity and response time for mainstream use in studies of physiological NO transport. Furthermore, many techniques are not capable of measuring NO at physiological levels near single cells or small organisms without the addition of labels or contact with the biological specimen. On the other hand, electrochemical probes and microprobes are quantitative, selective, rapid, and have little signal hysteresis. Thus, electrochemical probes persist as one of the leading technologies for measuring NO in complex solutions, and many recent papers have focused on techniques for enhancing electrochemical NO sensing.[15–18]

A number of research labs have demonstrated improved performance of electrochemical NO sensors by developing nanomaterial-functionalized electrodes. Specifically, these electrodes show enhanced conductivity, biocompatibility, and stability.[19–23] Although some of these electrodes have demonstrated detection limits in the nM range and response times on the order of milliseconds, inherent disadvantages include the need for external reagents, requirement of a large sensing area (with sensing area in the mm range), and inability to directly measure transmembrane flux. Zhang *et al.*[2] has resolved the issue of sensor miniaturization (probes as small as 500 nm were developed) and need for external reagents. To further extend this method, Porterfield *et al.*[24] developed a non-invasive NO microelectrode using a modality known as self-referencing (SR) as reviewed in detail by McLamore and Porterfield.[25]

The SR technique is a non-invasive method that allows direct measurement of microscale flux from a biological sample. Such non-invasive and reagent free techniques are vital for NO signaling, as physical contact with a cell/tissue or addition of exogenous reagents causes stress response signaling and induces bias in results. The SR microelectrode by Porterfield *et al.*[24] was based on a carbon fiber microelectrode (30 μm tip diameter) coated with *o*-phenylene diamine (OPD) and Nafion using the recipe by Friedemann *et al.*[26] The SR probe was used to measure NO flux as low as 1 pmol cm^{-2} s^{-1} from an individual macrophage cell, and also macrophage cell aggregates. NO flux was approximately ten times higher in cell aggregates, which highlights the ability of the SR technique to measure non-invasive flux with NO transport that correlates to cellular activity. Koehler *et al.*[27] later used this same technique to monitor NO release from photoactivated polymers and measured surface fluxes of approximately 14 pmol cm^{-2} s^{-1}. Although these carbon fiber sensors were effective, the probes are known to be difficult to reproduce, requiring specialized equipment (*e.g.*, microcapillary puller) and delicate handling (*i.e.*, electrolyte solution can leak at the carbon fiber seal). Furthermore, the sensor diameter in the work by Porterfield *et al.*[24] is relatively large (30 μm), limiting accurate spatial profiling of single cells and small organisms.

Based on the improvements in sensing O_2 radicals using nanoceria-graphene hybrid composites,[28] here, we report the development and application of a novel SR NO-selective microelectrode using a nanohybrid material to enhance sensitivity (see graphical abstract for schematic of nanohybrid material). In our previous work, this hybrid nanomaterial demonstrated excellent detection of oxygen radicals from xanthine oxidase (O_2^-) and glucose oxidase (H_2O_2).[28] The NO microelectrode was operated in the non-invasive SR modality for measuring NO flux in abiotic and living systems. Three distinct model living systems, with known NO signaling pathways, were used to test the effectiveness of the non-invasive NO sensor, including a microbial, animal (crustacean), and plant model. The microbial system targeted in this work is a lithifying biofilm known as a microbialite, which are one of the oldest known microbial ecosystems on Earth.[29] The model crustacean used in this study is *Artemia salina*, or brine shrimp, which is a primitive aquatic arthropod commonly used in developmental biology studies. Lastly, the model plant used in this study is *Arabidopsis thaliana*, a small flowering plant that is widely used as a model organism in genetics, molecular biology, and signaling. Together, these three model systems demonstrate the broad applicability and effectiveness of this novel microsensor in biological applications.

Methodology

Chemicals and materials for microelectrode preparation

Single layer graphene oxide (SLGO; 0.8 nm thickness, 1–5 μm diameter, 99% purity) was obtained from ACS Materials (Medford, MA). Methanol, sodium hypochlorite, ascorbic acid and lead acetate were purchased from Fisher Scientific (Atlanta, GA). Cerium(IV) oxide nanoparticle dispersion (12 nm, 10 wt% in H_2O; referred to as nCe throughout), and chloroplatinic acid (8 wt%) were procured from Sigma-Aldrich (St. Louis, MO). Nafion (5% aliphatic alcohol) and OPD were acquired from Acros organics (Newark, NJ). Nitric oxide gas (CP grade 99%) was purchased from AirGas (Gainesville, FL). Potassium ferrocyanide trihydrate ($K_3Fe(CN)_6$) and potassium nitrate (KNO_3) were purchased from EMD chemicals (Billerica, USA). Phosphate buffer saline (PBS) was purchased from Mediatech, Inc. (Manassas, USA). Parylene-insulated Pt/Ir microelectrodes (2 μm tip diameter, 5.1 cm length, 81 μm shaft diameter) were obtained from MicroProbes, Inc. (Gaithersburg, MD). Pt wire (99.95% Pt, 1.2 mm diameter, 2 cm length) for counter electrodes was obtained from Alfa Aesar (Ward Hill, MA). MAHMA NONOate and *S*-nitroso-*N*-acetyl-D,L-penicillamine (SNAP) were purchased from Sigma Aldrich (St. Louis, MO, USA).

Nanomaterial deposition

A composite of reduced graphene oxide (rGO), nanoceria (nCe), and nanoplatinum (nPt) was deposited on the tip of each Pt/Ir microelectrode based on the methods described by Chaturvedi *et al.*[28] and Vanegas *et al.*[30,31] First, rGO solution was

prepared by suspending SLGO in DI water at a concentration of 2 mg mL^{-1}, followed by ultrasonication with a tip horn sonicator (20 kHz) for 30 min. The SLGO was then reduced by immersing the probe in a solution of ascorbic acid (AA) (8 mg AA per mL) while baking at 60 °C for 45 min to produce rGO. Microelectrodes were rinsed in methanol, air dried for 10 min at room temperature, immersed in rGO suspension for 30 s, and then dried at room temperature for 20 min. Next, nPt was deposited on the rGO *via* sonoelectrodeposition (500 mHz) at 10 V for 30 s in a solution of 0.728% chloroplatinic acid and 0.002% lead acetate. A nCe layer was then formed on the rGO–nPt layer by immersion of the microelectrode tip in the nanoceria solution for 5 min, removing the microelectrode, and then air drying at room temperature for one hour. The microelectrode tip was then rinse in water three times and dried at room temperature for one hour. To facilitate charge exclusion of organic acids, a Nafion membrane was incorporated on top of the nanomaterial platform by dipping the tip of the microelectrode in Nafion solution for 20 min and then baking the electrode at 115 °C for 1 h. Finally, a size exclusion membrane was electrodeposited by polarizing the electrode at +900 mV in a solution of 5 mM OPD and 0.1 mM AA until output current showed less than 2% variability, approximately 120 min (see ESI Fig. S1†).

NO microelectrode characterization

The working principle for the NO microelectrode is based on oxidation of NO at the working electrode to nitrosonium cation (NO^+), which is then hydroxylated to nitrous acid (HONO) followed by deprotonation to nitrite (NO_2^-) (eqn (1)). Free electrons are detected as oxidative current *versus* a reference electrode at a constant oxidative potential.

$$NO \rightarrow e^- + NO^+ + OH^- \rightarrow HONO \rightarrow NO_2^- + H^+ \quad (1)$$

For calibration, NO stock solutions were prepared by either purging nitric oxide (gas) into PBS buffer (pH = 7.3) based on Porterfield *et al.*[24] or preparing stock solutions based on SNAP degradation.[2] *Warning: All nitric oxide standards must be prepared under a chemical hood and stored in a vial with syringe cap for calibration as nitrous oxide is a poisonous gaseous material.* In a previous study[32] we showed calibration of the electrode with NONOate for laboratory studies. In these field studies, use of NONOate was not possible due to lack of proper storage conditions (−80 °C). Calibration with NONOate is suggested (if possible) as the results are more reliable. For creating NO stock solutions by bubbling gas, stock solutions of 2 mM NO were created by bubbling dry argon through an airtight container of DI water for 30 min, and then NO gas was bubbled through the argon-purged water. For preparing SNAP standards, decomposition to NO was initiated by a Cu(I) catalyst, producing a stock solution of 0.1 mM NO (see ESI section and eqn (1) for details†). The NO stock solutions were stored in the dark when not in use; all SNAP calibrations were performed in the dark.

Methods for calibration and flux measurement were based on the approach described in detail by McLamore *et al.*[31] All measurements were performed at a constant working potential *versus* a Ag/AgCl reference electrode immersed in 3 M KCl and inserted into a half-cell microelectrode holder (World Precision Instruments, Inc., Sarasota, FL). For calibration, electrodes were polarized in PBS (pH = 7.3) and then NO stock solution was injected. Output current was monitored until the signal changed by less than 1%. Calibration curves were prepared using the steady state response for each step change and the reported sensitivity is the linear slope of the average output *versus* the NO concentration. All electrodes were calibrated before and after each biological experiment to ensure calibration drift did not induce bias in recordings of biological NO flux.

Response time was calculated for each stepwise addition of NO during calibration experiments using the methods in Chaturvedi *et al.*[28] Briefly, an exponential model was created and the model parameters were calculated by minimizing the chi^2 value for each step change. The model was then used to calculate the time associated with a 95% increase based on the recommendations by the International Union of Pure and Applied Chemistry (IUPAC). Limit of detection (LOD) was calculated using the 3-δ method, as described in Chaturvedi *et al.*[28] Selectivity was calculated as a percent change in sensitivity, as compared to the calibration for NO as described by McLamore *et al.*[33]

Abiotic transport studies

Calibrated NO microsensors were used to measure flux in the SR modality. The SR microsensor technique is a non-invasive modality that measures flux within the concentration boundary layer. SR uses computer-controlled translation of the microelectrode between two positions separated by a known distance (dX). Differential concentration (dC) is recorded in real time and flux is then calculated using Fick's first law of diffusion ($J = -D \times dC/dX$); where J = NO flux [nmol cm^{-2} s^{-1}], D = diffusion constant of NO [cm^2 s^{-1}], dC = NO concentration differential [nM], and dX = microelectrode oscillation distance [μm]. See McLamore and Porterfield[25] for a detailed review of the technique.

To prepare a stable abiotic NO concentration gradient for the abiotic transport studies, two different NO donor–polymer composites were injected into a source pipette based on McLamore *et al.*[34] and Koehler *et al.*[27] The polymers used in this study were chitosan, the major structural component of *Artemia* cyst shells as described by Tajik *et al.*[35] and alginate hydrogel, which has been used extensively as a material that mimics some of the properties of bacterial biofilms and tissues.[36,37]

Chitosan and alginate hydrogels were prepared according to Burrs *et al.*[38] NO stock solutions of 1 mM MAHMA NONOate were prepared in PBS, pH 7.3 and stored immediately when not in use at −80 °C. Composites of polymer and NO donor were prepared by mixing 1 mM stock NO donor solution with the polymer, vortex agitating for 30 s, and then immediately backfilling into a tapered borosilicate glass pipette (open diameter was 200 μm). The tapered pipette containing NO donor and polymer was immediately placed into a 3D micromanipulator (World precision Instruments, Sarasota, FL) with a resolution of 0.1 μm and immersed in PBS buffer. A calibrated NO microelectrode was positioned within 1 μm of the gel surface and flux was recorded based on the methods in McLamore *et al.*[33,34] For

all abiotic transport studies, NO concentration within 5 μm of the source pipette was validated using UV absorbance at 337 nm with a fiber optic UV spectrometer (Ocean Optics, Dunedin, FL) based on Koehler *et al.*[27]

A diffusion model was developed based on Koehler *et al.*[27] using eqn (2). NO diffusion coefficients vary considerably in different media, which can significantly affect flux data. For example, Koehler *et al.*[27] report a value of D (3.3×10^{-5} cm^2 s^{-1}) that is significantly higher than the value reported by Zacharia and Deen;[39] which is 2.21×10^{-5} cm^2 s^{-1}. To determine the effective diffusion coefficient (D_{eff}) in the polymer composite and conditions tested here, the deterministic model was used to calculate D_{eff} from empirical data by minimizing the chi^2.

$$C(x) = \frac{C_o R_o}{x} e^{\frac{-k(r-R_o)}{2D_{\text{eff}}}} \quad (2)$$

where: x = distance from tip of source pipette [μm]; C_o = concentration of NO in source pipette [120 nM]; R_o = radius of source pipette [200 μm]; k = rate constant for NO in solution [12 ms^{-1}].

Microbialite analysis in the intertidal zone

The microbialites were collected from the island of Highborne Cay located in the Exuma Sound, The Bahamas. Microbialites are carbonate build-ups formed by the metabolic activity of microbial mat communities. Microbialites are classified based on their internal structure and can range from laminated structures, known as stromatolites to unlaminated structures, referred to as thrombolites.[40,41] This work compared the NO profiles of stromatolites and thrombolites to assess whether different NO profiles correlate with known geochemical profiles for O_2, H^+, and HS^-. The methodology for measuring NO profiles in microbialites is based on Chaturvedi *et al.*[28] Spatially resolved NO depth concentration profiles were monitored throughout the diel cycle of each type of living microbialite. The two types of microbialites (stromatolite and thrombolite) were both juxtaposed in an intertidal zone with extensive wave activity, sand abrasion, and high levels of UV radiation. Microbialite samples were collected at midnight and noon, and then immediately returned to the field station for analysis. NO microsensors were mounted on a three-axis manual micromanipulator (World precision Instruments, Sarasota, FL) with a resolution of 0.1 μm. Microelectrodes were positioned at the mat surface, and concentration was recorded for 1 min. Sensors were then penetrated into the mat and concentrations were recorded every 200 μm to a total depth of 1.6 mm. Profiles were collected (in triplicate) for three different microbialites (total n = 9). All studies were conducted during July of 2014.

Electrochemical measurements for the microbialite studies were performed on a handheld potentiostat with integrated impedance analyzer (PocketSTAT, Ivium technologies, Eindhoven, Netherlands). Electrical impedance spectrographs (EIS) were analyzed before and after each experiment to ensure microelectrodes were undamaged using a solution of 4 mM $KFe(CN)_6$/100 μM KCl with an applied potential of 100 mV (AC) and 0.25 mV (DC) within the frequency range of 1 Hz to 100 kHz. Pt wire was used as a counter electrode and reference electrodes were constructed as described in McLamore *et al.*[32] using Ag/AgCl wires immersed in 3 M KCl with 1% agar contained in a polystyrene tube (1.5 mm diameter). DC potential amperometry (DCPA) measurements in field samples were conducted with a three electrode setup based on Dupraz *et al.*[40] Electrodes were polarized in seawater for at least 1 h, and current was measured at constant potential while profiling all mats. For each position within the profile, output current was measured until the signal reached steady state (less than 5% deviation) while recording at a sample rate of 120 Hz.

Artemia cyst development

Artemia salina is a primitive aquatic arthropod that reproduces using encysted gastrula embryos (cysts). *A. salina* are commonly used in developmental biology studies focused on environmental resilience.[42] Grade A encysted *A. salina* embryos (cysts) were obtained from Brine Shrimp Direct (Ogden, UT), and were stored at 4 °C when not in use, as described by Van Stappen.[43] Cysts were hydrated in filtered seawater obtained from the Whitney Marine Biosciences Laboratory at the University of Florida based on Heffer *et al.*[44] Immediately after hydrating cysts, hatching assays were conducted based on Clegg[45] in filtered seawater at 22 ± 3 °C to confirm viability; 98 ± 3% of the cysts hatched in seawater (n = 50). Diapause cysts were hydrated and used directly as non-decapsulated (ND) embryos. For decapsulated (DC) *Artemia* cyst experiments, the cyst shell was removed based on Veeramani and Baskaralingam.[46] Briefly, *Artemia* cysts were immersed in sodium hypochlorite solution (11% w/w) for 30 min, and DC cysts were then washed with DI water in a nylon mesh filter (100 μm) for 30 min.

The methods for measuring NO flux were based on work by Stensberg *et al.*[47,48] which used ion probes for monitoring physiological signaling in developing *Daphnia magna* embryos. In this work, *Artemia* cysts (both ND and DC) were placed in a 10 mL micro Petri dish in buffer at 25 °C and placed on a vibration isolation table containing a microscope and the SR microelectrode hardware. Cysts were observed under the microscope to ensure they were fully hydrated or decapsulated in the case of DC cysts. Once a minimum of 15 hydrated ND or DC cysts were identified, a calibrated NO microelectrode was then positioned within 1 μm of the embryo surface using the camera/zoomscope apparatus and 3D motor controlled stages, and flux was recorded by oscillating the electrode in the direction perpendicular to the tangent of the embryo surface.[47,48] The excursion distance for all experiments was 20 μm and the oscillation frequency was 0.30 Hz. After recording baseline NO flux for at least 10 min, 5 mM H_2O_2 was added to the dish and the NO flux continuously recorded. Control experiments were conducted with no cysts to remove signal bias due to addition of exogenous H_2O_2.

Arabidopsis thaliana ovule stress signaling

Two *A. thaliana* genotypes were selected for these experiments: per17 mutants and wild-type plants (Col-0 ecotype). Previous work showed that per17 mutants produce copious amounts of

seeds when grown under normal growth conditions, but ovules in these plants can be induced to undergo seed failure or ovule abortion at a high frequency when plants are stressed by watering with 75 mM NaCl.[49]

After 37 days, siliques were approximately 8–10 mm in length, and 400–600 μm in diameter. Photographs of the plants after 37 days of growth and also photographs of a microsensor at the surface of a Col-0 ovule are shown in ESI Fig. S2.† The silique wall was carefully opened using Dumont #6 forceps (EMS, Hatfield, PA) under a dissection microscope. After opening the silique wall, plants were placed on the vibration table and prepared siliques were fixed to the base of a 10 mL Petri dish using adhesive putty. An 8 mL aliquot of 0.1 M MS solution, containing 20.6 mM NH_4NO_3, 0.1 mM H_3BO_3, 4.0 mM $CaCl_2$, 0.1 μM $CoCl_2$, 1.5 mM $MgSO_4$, 0.1 μM $CuSO_4$, 1.2 mM KH_2PO_4, 0.1 mM $FeSO_4$, 18.8 mM KNO_3, 0.1 mM $MnSO_4$, 5.0 μM KI, 1.0 μM Na_2MoO_4, and 30 μM $ZnSO_4$ was added to the dish. SR NO microsensors were immediately positioned within 1 μm of the seed ovule surface, and NO flux was measured for at least 5 min per ovule. At least three ovules in each silique were measured in triplicate, with at least 9 total ovules per genotype.

Statistics

All measurements were performed in at least triplicate. Analysis of variance (ANOVA model I) or one-tailed student's *t*-test was used to test for significance as noted. All error bars represent standard deviation of the arithmetic mean, and values of *n* are reported for each data set.

Results and discussion

Nitric oxide sensitivity

The sensitivity of each electrode toward NO in PBS (pH = 7.3, 25 °C) for various nanomaterial composites is shown in Fig. 1. While the addition of a single nPt, rGO or nCe layer to the electrode surface increased sensitivity, the combination of nPt and rGO did not increase sensitivity. This highlights the importance of the nCe layer in the membrane for oxidation of NO. The hybrid material containing all three nanomaterials (group d, Fig. 1) was more sensitive to NO than rGO, nCe, nPt, nPt–rGO, or rGO–nCe coated electrodes (groups a–c). This is similar to our previous studies of oxygen radical sensing,[28] where hybrid nanomaterials containing platinum, rGO and nanoceria are significantly more sensitive than other combinations of the nanomaterials. Representative calibration curves can be seen in Fig. 1a and average calibration curves are shown in Fig. 1b. When coated with Nafion and OPD, the sensitivity decreased by approximately 4%, but these materials are absolutely necessary for size and charge exclusion permitting these sensors to be selective for NO in biological applications. For the rGO–nPt–nCe nanohybrid microelectrode, the sensitivity was 0.95 ± 0.03 pA nM^{-1}, the LOD was 0.9 ± 0.3 nM (SNR = 3), and the response time was 1.1 ± 0.1 s. Response time and LOD showed similar trends as the average sensitivity data shown in Fig. 1b, confirming that the rGO–nPt–nCe arrangement had the best performance while the nCe-coated electrode had the poorest performance among the materials tested. A comparison to other current microelectrodes and discussion of the limitations and advantages of this material for physiological sensing is presented in Table 1 and related discussion.

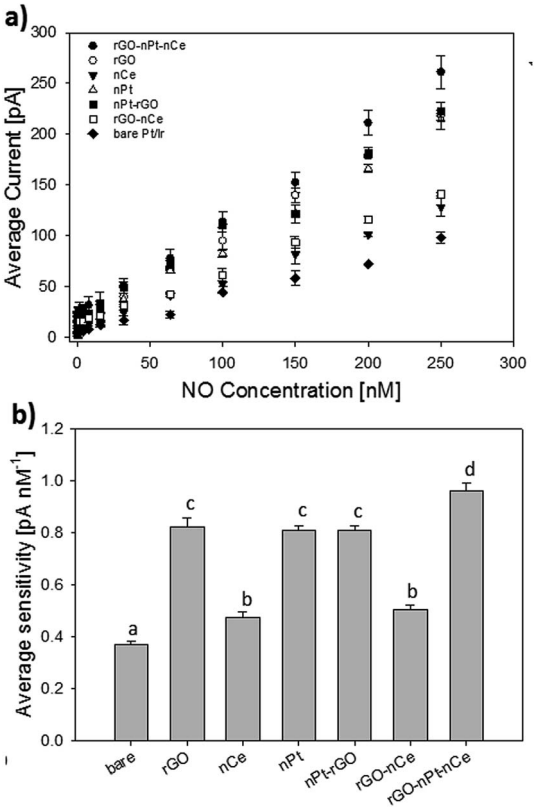

Fig. 1 Effect of nanomaterials on NO sensitivity in PBS (pH = 7.3 at 25 °C) using both SNAP ($n = 3$) and NO(g) stock standards ($n = 3$). (a) Average calibration plots for various hybrid materials on a 2 μm Pt/Ir electrode. All hybrid materials were coated with Nafion and OPD. (b) Average sensitivity for all microelectrodes ($n = 6$). Lower case letters represent groups with statistical difference based on ANOVA ($\alpha = 0.05$).

As discussed by Xu and Qu[50] and also Joung *et al.*[51] cerium oxide nanoparticles (*i.e.*, nanoceria) have received significant attention as a biocompatible catalyst due to the quick and expedient transition between Ce^{4+} and Ce^{3+} oxidation states. Furthermore, nanoceria has tunable defect sites in the lattice structure that can be engineered to mimic the chemical reactivity of enzymes, including superoxide oxidase, catalase and oxidase.[52] By combining the catalytic properties of partially reduced graphene oxide and nanoplatinum together with nanoceria, we have developed a highly efficient NO microelectrode. Scanning electron micrographs and electron dispersive X-ray spectroscopy confirm the formation of distinct stratified layers of rGO, nPt, and nCe on the electrode surface (see ESI Fig. S3†).

The faradaic current as a function of polarization potential is shown in ESI Fig. S4.† At an oxidative potential below +500 mV the current was not measureable *versus* a Ag/AgCl reference electrode. Above +650 mV, an oxidative current was detectable,

Table 1 Comparison of NO-selective electrochemical microelectrodes (tip size smaller than 100 μm) within the last 15 years in terms of response time, sensitivity, operating potential, and limit of detection[d]

	Coating/membrane	Potent. [mV]	Diam. [μm]	Res. time [sec]	Sensitivity	LOD (nM)	Reference
Carbon fiber	WPI membrane[a]	+865	7	3 ± NR	0.5 ± NR, pA nM^{-1}	2.0 ± NR[b]	Zhang *et al.* (2002)
	Nafion and cellulose acetate	+870	6[c]	4 ± NR	0.3 ± NR, pA nM^{-1}	1000 ± NR	Katrlik *et al.* (2002)
	DOW Corning® membrane	+720	30–40	1 ± NR	0.002 ± NR, pA nM^{-1}	30 ± NR	Schreiber *et al.* (2008)
	Nickel porphyrin	+830	7	≈30 ± NR	0.8 ± NR, pA nM^{-1}	1.5 ± NR	Hrbác *et al.* (2006)
Pt electrode	Nafion and WPI membrane[a]	+865	50	10 ± NR	5.8 ± NR, pA nM^{-1}	2.1 ± NR	Dickson *et al.* (2004)
	Nano Pt	+750	150	25 ± NR	0.8 ± NR, pA nM^{-1}	0.1 ± NR	Lee *et al.* (2004)
	Nano Pt	+850	25	14 ± NR	0.4 ± 0.1, pA nM^{-1}	1.0 ± NR	Lee *et al.* (2007)
	Permiselective fluorine modified xerogel	+800	20	3 ± NR	7.9 ± NR, pA nM^{-1}	0.1 ± NR	Shin *et al.* (2008)
	Nanoceria-graphene composite, Nafion, OPD	+720	2	1.1 ± 0.1	0.95 ± 0.1, pA nM^{-1}	0.9 ± 0.3	This work

[a] Material details patented by World Precision Instruments. [b] SNR of 2 was used to calculate LOD value. [c] Manuscript reports an electrode bundle (6–10 electrodes). [d] NR = not reported.

and maximized at approximately +900 mV (see ESI Fig. S4†). These results are similar to the trends by Zhang *et al.*[2] where no stable plateau was attained, indicating that NO diffusion limited transport at high overpotential. Importantly, the overpotential at which faradaic current was detected for the rGO–nPt–nCe microelectrode (+720 mV) was significantly lower than Zhang *et al.*[2] (+865 mV). However, direct comparisons of these two sensors are difficult due to differences in tip diameter and membrane thickness. However, the results in Fig. S4† show an average increase in faradaic current for the hybrid sensor of approximately 55% compared to a bare Pt/Ir microelectrode. Furthermore, the overpotential of our nanohybrid sensor (+720 mV) is significantly lower than a bare Pt/Ir electrode (+865 mV). The underlying mechanism of the relatively low overpotential in our study is the rapid oxidation of NO to nitrosonium cation as a result of the synergistic electrokinetic effect of the rGO–nPt–nCe nanohybrid composite. Lee *et al.*[53] showed a low overpotential for nPt-modified electrodes (+750 mV). Furthermore, Miao *et al.*[54] showed that NO can be oxidized at +700 mV on glass carbon electrodes (2 mm diameter) polymerized with *o*-aminophenol and palladium nanoparticles. Liu *et al.*[21] showed that drop cast (*i.e.*, porous) graphene electrodes with intermediate degrees of reduction and high Raman I_D to I_G peak ratios exhibit an NO oxidation peak potential at +764 mV.

Selectivity study

Although the overpotential of the nanohybrid sensor is an improvement over previous designs, oxidation of other compounds at +720 mV is a major problem in NO sensing, particularly when considering the rapid oxidation of NO. A membrane containing Nafion (for charge exclusion) and OPD (for size exclusion) on the outermost layer of the electrode is the most common approach for improving selectivity. Using this approach, the rGO–nPt–nCe microelectrode showed excellent selectivity over ascorbic acid (765 : 1) and nitrite (940 : 1) in PBS (pH 7.3 at 25 °C) (see ESI Table S1† for details). The selectivity over ascorbic acid is higher than previous reports for OPD and Nafion on carbon fibers (600 : 1 for AA and 900 : 1 for NO_3).[26] This improvement is likely due to the relatively low overpotential used in our study (+720 mV) as ascorbic acid and nitrite oxidize at a potential of approximately +800 mV. The hydrophobicity of the outer OPD membrane may have also contributed to the high selectivity in our design, as Zhang *et al.*[2] showed that hydrophobic membranes improve selectivity toward NO in the presence of dopamine, serotonin, nitrite, L-arginine, and AA. Interference by carbon monoxide (CO) is a possible issue regarding signal interference, but in these studies we did not use a secondary test to confirm CO levels in the field studies.

Many manuscripts have described techniques for limiting interference by oxidizeable biological molecules used in NO sensing.[55] However, one of the major problems for electrochemical NO sensors rarely discussed is interference by reactive oxygen species (ROS), such as H_2O_2 and O_2^- that oxidize at potentials of approximately +685 mV. Although our relatively low overpotential (+720 mV) is an enhancement, the problem of ROS oxidation, specifically H_2O_2 and O_2^-, is a persistent problem. This issue is a major challenge in the field of NO sensing, and new membrane materials that can facilitate rapid oxidation of NO, while limiting interaction with O_2^-, H_2O_2 and dissolved oxygen are sorely needed.

Comparison of various NO electrodes

Table 1 shows a comparison of NO-selective electrochemical microsensors that have either been used in field studies or are applicable for field studies. While there are many other NO sensors which have been used in laboratory studies not shown in Table 1, this summary compares only the devices that are relevant to biological applications similar to the data shown in Fig. 3–5. The sensitivity (0.95 ± 0.03 pA nM^{-1}), response time

(1.1 ± 0.1 s), operating potential (+720 mV), and selectivity for the nanomaterial-modified Pt microelectrode (2 μm tip diameter) are all similar to previous microsensor designs (Table 1). The LOD of our sensor (0.9 ± 0.3 nM) was within the appropriate range for physiological studies based on previous measurements with paramagnetic resonance. Although our microelectrode shows excellent performance, selectivity over other oxygen radicals persists as a major problem, which is particularly challenging for field experiments as shown here. Each of the electrodes in Table 1 exhibited signal bias due to the presence of oxygen and oxygen radicals, including H_2O_2 and O_2^-, which oxidize at an overpotential lower than NO. Furthermore, these species are known to rapidly degrade dissolved NO in solution, which is enhanced in the boundary layer near the electrode surface due to the high oxidative potential. There are a number of techniques that have been developed for enhancing NO sensor performance that could not be used for the biological applications herein (particularly the marine biology studies were research permits are required). For example, Wu *et al.*[56] describe methods used to account for temperature artifacts and interference by non-target compounds using a gallium arsenide sensor, which was not allowed for use in the open ocean near a protected coral system due to the possibility of arsenic release.

One of the first successful electrodes was the design by Friedemann *et al.*[26] which was a 30 μm carbon fiber coated with OPD and Nafion. The response time (0.5 s) and selectivity (1 : 765 for AA and 1 : 940 for and nitrite) are similar to many current designs. However, the last decade has seen significant improvements in sensitivity, limit of detection, and overpotential for smaller electrode designs. As discussed by Katrlik *et al.*[57] carbon fiber electrodes have been prepared by coating the electrode with a wide array of other materials to impart selectivity toward NO, including: electro-polymerized Ni-porphyrin, poly(4,4′-dihydroxybenzophenone), cellulose acetate, polydimethyl-siloxane, and polystyrene. Hrbác *et al.*[58] developed a nickel-porphyrin coated carbon fiber NO electrode (7 μm diameter) with a high selectivity towards NO over nitrite (1 : 600) and ascorbate (1 : 8000) at +830 mV. The sensitivity at +830 mV was relatively high (0.825 pA nM^{-1}) with a response time of approximately 30 s and a LOD of 1.5 nM. Katrlik *et al.*[57] also developed a relatively small carbon fiber electrode (6 μm) containing a Nafion and cellulose acetate membrane with a sensitivity (0.34 pA nM^{-1}) and response time similar to other electrodes, although detection limit (1 μM) and selectivity were poor, limiting the applications for studies of physiological NO transport. Zhang *et al.*[2] developed one of the most successful carbon fiber microelectrodes (as small as 500 nm tip diameter) with a sensitivity of 0.5 pA nM^{-1}, an LOD of 2.0 nM, and response time of 3 s. However, this LOD was calculated based on a signal to noise ratio (SNR) of 2, which is relatively poor; when we calculated the LOD of the rGO–nPt–nCe microelectrode based on a SNR of 2, the value was significantly lower (0.9 ± 0.3 nM) than Zhang *et al.*[2]

Platinum (or platinum/iridium) electrodes are also commonly used to develop NO microelectrodes (see Table 1). Lee and Kim[59] developed a nPt-modified Pt micro electrode (25 μm) coated with poly-tetrafluoroethylene (PTFE) with a sensitivity of 0.39 ± 0.03 pA nM^{-1}, a response time of 14 s, and a LOD of 1 nM at a potential of +850 mV. In a similar study, Lee *et al.*[53] developed a nPt-modified platinum microelectrode (150 μm tip diameter) covered with a microporous PTFE membrane and a NO-selective membrane developed by World Precision Instruments (details of the material properties are patent protected). The sensitivity of the electrode toward NO(g) was 0.8 pA nM^{-1}, with a response time of 25 s and a LOD of ≈1 nM. When accounting for the large electrode surface area for the electrode developed by Lee and Kim,[59] these improvements are minor, the former electrode was three times larger than Lee *et al.*[53] Dickson *et al.*[60] developed an extremely sensitive flexible Pt microelectrode (50 μm) with a sensitivity of 5.76 pA nM^{-1}, the overpotential was +865 mV, response time of 10 s, and LOD of 2.1 nM. One of the most promising Pt microelectrodes is the design by Jae *et al.*[55] This Pt electrode was coated with a permiselective fluorine-modified xerogel polymer. The microsensor (20 μm) had a sensitivity of 7.91 pA nM^{-1}, response time of 3 s, LOD of 83 pM, and excellent selectivity over common interferents such as nitrite, ascorbic acid, uric acid, acetaminophen, dopamine, ammonia/ammonium, and carbon monoxide. The only disadvantage of this electrode was the relatively large size (20 μm) and the relatively high overpotential (+800 mV).

Recently, a number of groups have developed nanomaterial-mediated electrodes for NO sensing. However, most of these nanomaterials have not yet been used to develop microelectrodes that can be used in studies of physiological NO flux at the single cell or small organism scale. Li *et al.*[19] developed a nanogold-decorated graphene hydrogel composite with Nafion on a glassy carbon electrode and showed that the hybrid nanomaterial resulted in an increased faradaic current approximately five times higher than gold nanoparticles alone, and an electroactive surface area approximately six times higher. The response time (3 s), sensitivity (45 nA μM^{-1}), and LOD (9 nM) are all excellent. However, direct comparison to the microelectrodes in Table 1 is not feasible since Li *et al.*[19] used a 3 mm glassy carbon electrode. Although this device was not a microsensor, it demonstrates the effective use of metal-decorated graphene as the sensing layer in NO sensors. Further work is needed to understand the effect of pH on this design for physiological analyses, as this work showed strong dependence of faradaic current on pH in the range of 6.5 to 8.5.

Abiotic transport studies

Prior to application of NO sensors in biological applications, abiotic transport studies were conducted to validate the SR sensors. For each experiment, eqn (1) was used to calculate the effective diffusion coefficient D_{eff} of a polymer–NO donor composite. The NO efflux from each polymer composite is shown in Fig. 2. In each experiment, the pipette tip diameter was 200 μm. The NO flux followed Fick's first law ($\varepsilon > 0.98$) for both polymers. All concentration profiles measured within the unstirred layer near a source pipette followed Fick's first law based on eqn (1) (see ESI Fig. S5 for details†). 10 min after immersion in PBS buffer the concentration at that source pipette was within 2% of values obtained with a fiber optic UV

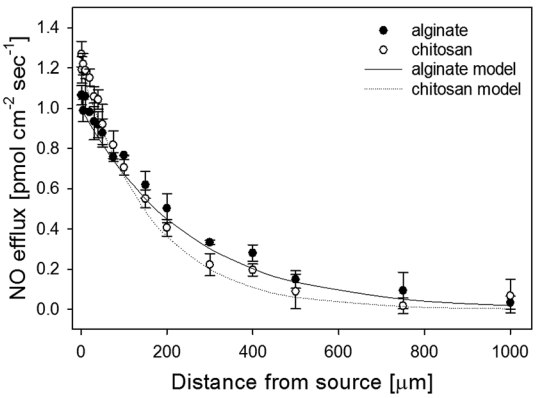

Fig. 2 Average abiotic NO flux from source pipette (200 μm tip) containing 1 mM MAHMA NONOate in hydrogels composed of chitosan, and alginate ($n = 3$). A first order Fickian transport model was used to calculate the effective diffusion coefficient (D_{eff}) each hydrogel. D_{eff} for chitosan (2.09×10^{-5} cm^2 s^{-1}) was not significantly different than alginate (2.05×10^{-5} cm^2 s^{-1}); $p < 0.001$, $\alpha = 0.05$.

spectrometer (337 nm). The flux values were similar to NO efflux from MAHMA NONOate entrapped in cellulose nanocrystal hydrogels,[61] and various hydrophobic polymers,[62] which ranged from approximately 1 pmol cm^{-2} s^{-1} to 100 pmol cm^{-2} s^{-1}. However, the flux values were approximately an order of magnitude lower than Porterfield *et al.*[24] using a SR carbon fiber electrode and SNAP agarose gels. Although differences in NO donor and gel properties may have contributed to these discrepancies, the inconsistency is more likely the difference in temperature. Porterfield *et al.*[24] performed studies at 37 °C, while our tests were all conducted at 25 °C. As noted by Mowery and Meyerhoff,[61] plasticizer weight and hydrophobicity also play major roles in NO release from polymer composites.

The D_{eff} value for chitosan (2.09×10^{-5} cm^2 s^{-1}) was not significantly different than alginate (2.05×10^{-5} cm^2 s^{-1}). These D_{eff} values were similar to the diffusion constants reported by others, 3.3×10^{-5} cm^2 s^{-1} and 2.21×10^{-5} cm^2 s^{-1} reported by Koehler *et al.*[27] and Zacharia and Deen,[39] respectively. Dickson[60] showed that values of D_{eff} for NO in polymers vary significantly based on the weight percent of plasticizer; from 2.5×10^{-6} cm^2 s^{-1} for low weight percent plasticizer films to 3.0×10^{-5} cm^2 s^{-1} in silicone films. The important differences when comparing our results to other studies were differences in gel thickness, surface chemistry, and gel pore size. Mowry and Meyerhoff[61] used a 200 to 300 μm thick plastic film and monitored transport of gas phase NO between equilibrium chambers. In addition to the difference in material properties (hydrophobicity, pore size), the Mowery and Meyerhoff system measured gas phase NO rather than dissolved NO, as in our studies. Future studies directly using these constants with different polymers must carefully consider dissolution of NO from MAHMA NONOate, pore size, hydrophobicity and gel thickness.

Spatial profiling of NO gradients in a marine microbialite system

NO depth profiles were monitored in two types of lithifying microbialites located in the shallow waters of Highborne Cay, The Bahamas (Fig. 3). Each type is distinguished by the internal carbonate structures with thrombolites having a clotted, or unlaminated appearance and stromatolites having a laminated structure (Fig. 3a and b).[63,64] In both of the microbialite types there was a significance difference in NO profiles throughout the diel cycle based on ANOVA (Fig. 3c and d). In thrombolites, the average NO concentration at the surface at noon (7.8 ± 0.5 nM) was significantly higher than the surface concentration at midnight (2.6 ± 0.1 nM); $p < 0.001$, $\alpha = 0.05$. Within the upper 250 μm of the mat, NO concentration increased by 68 ± 8% at noon, but the dropped sharply to a concentration of 1.0 ± 0.3 nM at a depth of 1.5 mm. At midnight, the NO increase with depth was more gradual, and reached 60% higher than the surface NO concentration. At a depth of 1.5 mm the NO concentration at midnight was 5.8 ± 0.1 nM.

A similar trend was seen in the stromatolites, with the average NO concentration at the surface of stromatolite mats at noon (13.3 ± 0.5 nM) was significantly higher than the surface concentration at midnight (3.0 ± 0.5 nM); $p < 0.001$, $\alpha = 0.05$. At noon, NO concentration increased by 36 ± 13%, within the upper 250 μm of the mat, but sharply decreased to a concentration of 6.7 ± 1.1 nM at a depth of 1.5 mm. At midnight, the NO profile was similar to the thrombolite mats, and gradually increased to a concentration of 6.0 ± 0.2 nM at a depth of 1.5 mm.

The precise function of NO in the microbialites is not clear, however, NO has been shown to mediate a wide range of functions in marine organisms[65] that includes, but is not limited to, cell growth,[66] symbiosis,[67] cell–cell communication,[68] and regulation of carbon and nitrogen assimilation.[69] The diel flux of NO in the microbialites likely reflects the natural diel cycling of the metabolic activities, which form distinct geochemical gradients throughout the depth profile.[40,70]

Although there are numerous microbial pathways that lead to NO formation (for a review see Schreiber *et al.*[71]), few occur under oxic conditions. In the upper zone (0 to 3 mm) of the microbialite there are high gradients of oxygen with concentrations ranging up to 900 μM.[40,41,70,72] Previous studies have shown that the primary metabolisms associated with NO production in oxic zones of marine sediments are typically nitrifying organisms, such as nitrite oxidizing bacteria, ammonia oxidizing bacteria.[71] However, metagenomic analyses of the thrombolite forming microbial communities have identified few nitrification genes.[41] Metatranscriptomic analyses of the thrombolites, however, have recovered several transcripts associated with flavoredoxin/nitrogen oxygen synthesis localized to the upper 3 mm of the thrombolites. These recovered genes share sequence similarity to coccoid cyanobacteria.[72] Unfortunately, no comparable metatranscriptomic database exists for the adjacent stromatolites. Additional examination of changes in the transcriptome over spatial and diel scales in both microbialite types will be required to fully assess the mechanisms associated with the formation and function of NO in lithifying microbial communities.

NO flux during brine shrimp development

NO flux was measured for non-decapsulated (ND) and decapsulated (DC) *Artemia salina* (brine shrimp). *Artemia* is a model

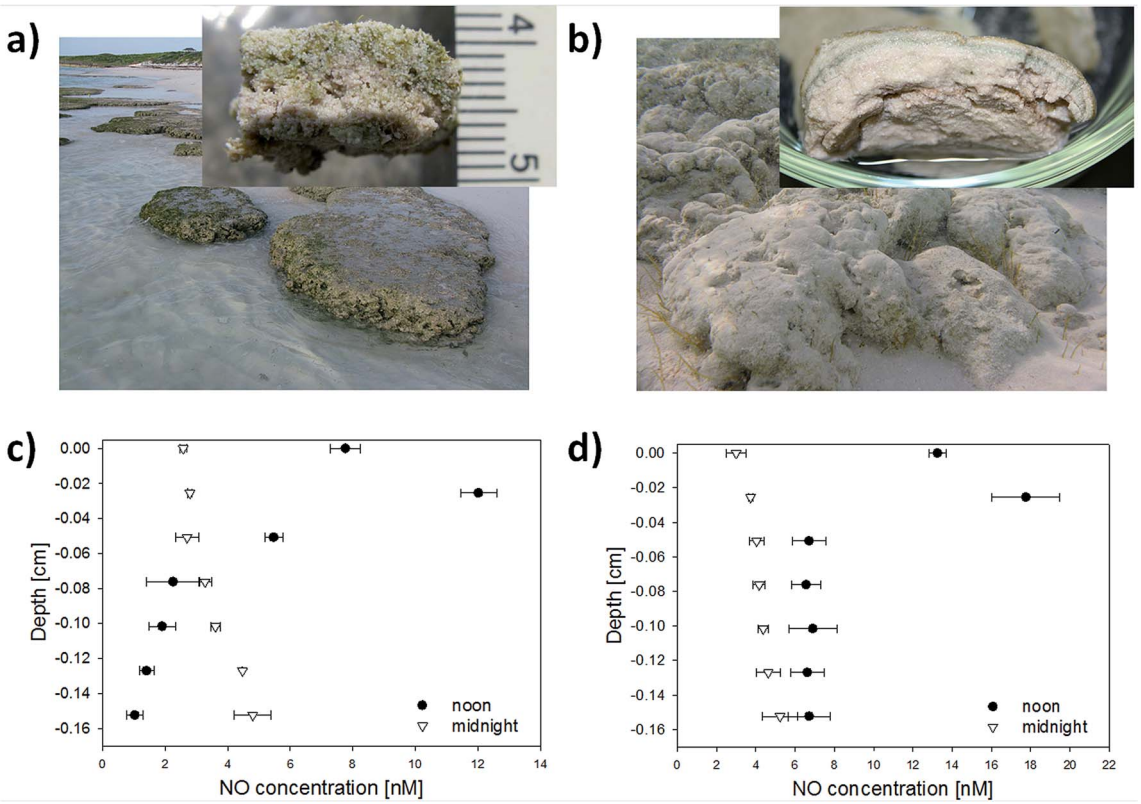

Fig. 3 NO microsensor profiles of marine microbialites derived from the island of Highborne Cay located in the Exuma Sound, The Bahamas. Photographs of (a) thrombolites, and (b) stromatolite; insets show microscopic structure. The average NO depth profiles are shown for (c) thrombolites and (d) stromatolites.

animal (crustacean) organism commonly used in developmental biology studies. Within 5 min of H_2O_2 addition (5 mM), the surface concentration of NO began to increase in ND cysts, but not in DC cysts (Fig. 4; see ESI Fig. S6† for concentration data). After 30 min of exposure to H_2O_2, the average surface NO concentration in ND cysts (9.3 ± 1.1 nM) was significantly higher than in DC cysts (1.1 ± 0.3 nM) ($p < 0.001$). This result is similar to the results by Veeramani and Baskaralingam[46] using spin trap EPR, although no concentration data was inferred from the EPR analysis. Fig. 4 shows the NO flux data for ND and DC cysts, respectively, which is a much more sensitive measurement than surface concentration as described by McLamore and Porterfield (2011).

The life cycle and embryonic developmental stages of *Artemia* depend strongly on salinity. In the cyst stage, *Artemia* (typically 200–250 μm in diameter) exists in a state of obligate dormancy called diapause, which can be terminated by specific environmental stimuli. Post-diapause development results in emergence of nauplii.[73–75] One of the reasons this organism is used in developmental biology studies is that diapause cysts are composed of ~4000 cells that are arrested at the G2/M phase and RNA and protein synthesis are completely dormant.[42] NO has been shown to play a critical role in the regulation of diapause termination and also post-diapause development in *Artemia* cysts.[76] Our results are in agreement with those reported by Robbins *et al.*[76] who showed that exogenous H_2O_2 promotes cyst development, emergence, and hatching, which is maximized at concentrations of 100 nM for an exposure time of 4 h.

NO synthesis has also been suggested to play a protective role in shell-bound iron-mediated ROS generation by acting as an iron chelator.[46,77] Veeramani and Baskaralingam[46] suggested that shell-bound iron plays a critical role in triggering NO formation to counteract the adverse effects of ROS-mediated stress during diapause deactivation. Liu *et al.*[42] found that low iron levels in the shell are linked to downregulation of the shell gland gene known as SGEG. Another possible connection to the enhanced NO flux in ND cysts may be related to 5′ adenosine monophosphate (AMP) activity. Post-diapause development in *Artemia* cysts is a complicated process involving a variety of metabolic and biochemical events. During post-diapause stages, *Artemia* cysts are known to produce large amounts of AMP-activated protein kinase (AMPK), a regulator of energy homeostasis.[42,77,78] Although a major role of AMPK in cells is to regulate erythropoietin-mediated activation of nitric oxide synthase (eNOS),[79,80] direct evidence of the link between eNOS and AMPK for inducing NO formation to counteract the adverse effects of ROS-mediated stress during diapause deactivation has not been studied in detail. In future studies, the non-invasive NO sensor shown here can be used for hypothesis testing related to the physiology of arrested development.

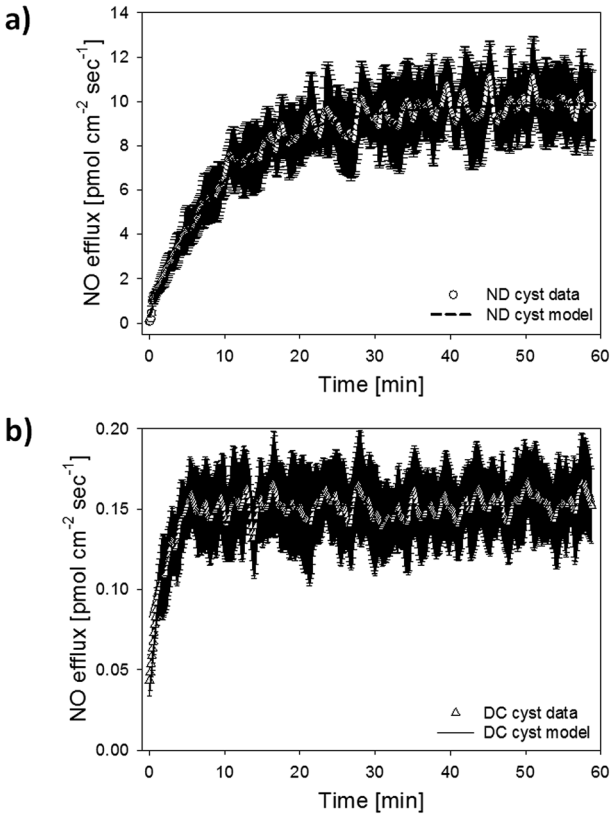

Fig. 4 Average NO efflux ($n = 15$) recorded at the surface of developing (a) non-decapsulated cysts (ND) and (b) decapsulated cysts (DC) of *Artemia salina* (brine shrimp) after exposure to 5 mM H_2O_2.

NO flux in developing *A. thaliana* ovules

NO efflux from developing ovules was measured in two genotypes of *A. thaliana*. The ovules were measured under non-stressed and stressed conditions while intact within the silique. In unstressed *per17* mutants, 31% of the seeds undergo seed failure, while in salt-stressed plants the seed failure rate doubles to 66%.[49] Correlating with this change in fecundity, the average NO surface concentration near ovules from *per17* mutants was significantly higher ($p < 0.001$) for stressed ovules (6.2 ± 2.1 nM) compared to non-stressed ovules (1.1 ± 0.2 nM). Likewise, the average NO efflux for *per17* stressed ovules (0.72 ± 0.18 pmol cm^{-2} s^{-1}) was significantly higher ($p = 0.026$) than non-stressed ovules (0.51 ± 0.28 pmol cm^{-2} s^{-1}) (Fig. 5a). In wild-type controls, the baseline surface concentration of NO (1.4 ± 0.3 nM) and efflux (0.62 ± 0.18 pmol cm^{-2} s^{-1}) was significantly lower than stressed ovules (28.2 ± 0.9 nM, and 2.56 ± 0.15 pmol cm^{-2} s^{-1}, respectively). The average seed failure for control plants was 13%, and the trace NO efflux data for control plants is shown in Fig. 5b. Prior to NO analysis, none of these ovules exhibited morphological symptoms of abortion. Thus these data are consistent with NO being a signaling molecule in the seed abortion pathway.

NO is known to play a role in seed development, and *A. thaliana* has been used as a model organism in many previous studies.[81] Reduction in fertility often results from ovule abortion and embryo senescence.[82] Furthermore, NO is known to play an important role in seed development such as initiation of signaling cascades that lead to synthesis of redox sensitive proteins (RSP).[83] RSP regulate photosynthetic and respiratory oxygen to balance radical production and cue appropriate cellular responses during stress. Delledonne *et al.*[84] showed that NO may act as a defense signaling molecule during seed germination. Furthermore, Bethke *et al.*[81] showed that NO can increase germination rate in *A. thaliana* (Col genotype). In Bethke's work, the effect was concentration dependent and reversed by addition of the NO scavenger 2-(4-carboxyphenyl)-4,4,5,5-tetramethylimidazoline-1-oxyl-3 oxide (cPTIO).

Our studies demonstrate that the NO microelectrode is a viable tool for exploring the underlying signaling mechanisms related to seed abortion. Although we focus our studies on NO signaling in ovules, the technique can potentially be used for hypothesis testing in many other plant tissues. For example, NO signaling has been linked to germination, growth rate of pollen tubes, stomatal movement, programmed cell death,[9] disease resistance,[7] and stress response,[6] and recent reviews describe the role of NO in complex signaling cascades in *A. thaliana*.[85]

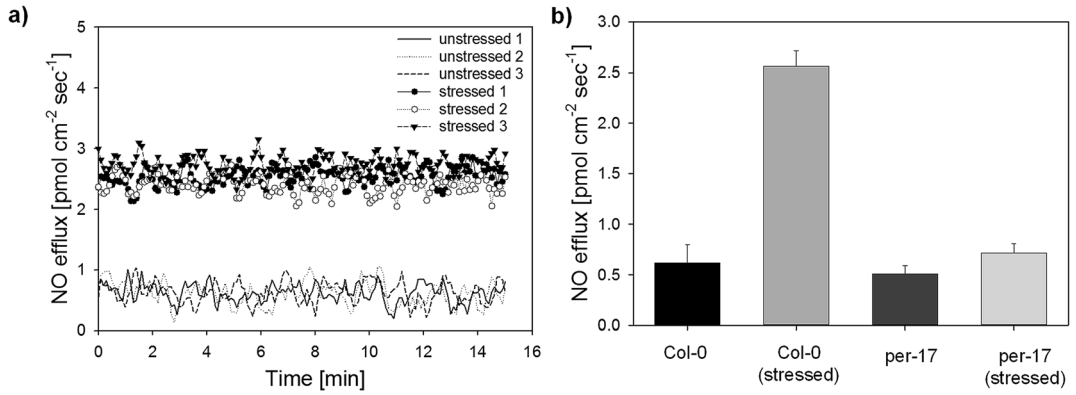

Fig. 5 Average NO efflux for stressed and unstressed *A. thaliana* ovules ($n = 15$). NO flux was significantly higher in plants which were salt stressed, demonstrating the protective role of NO in stress response.

Conclusions

We developed a high performance microsensor technique for real-time determination of NO concentration and flux in biological systems. The detection mechanism is based on the oxidation of NO at the surface of an electrode polarized at a low overpotential (+720 mV). Significant enhancement on performance was achieved after incorporation of an rGO–nPt–nCe platform on the surface of the electrode. The microsensor exhibited a high sensitivity (0.95 ± 0.1 pA nM^{-1}), fast response time (1.1 ± 0.1 s), and low detection limit (1.8 ± 0.3 nM). Charge and size exclusion of interferent molecules was ensured through inclusion of Nafion and OPD membranes on top of the nanomaterial platform, providing excellent selectivity towards NO. The microsensor was operated in the SR mode for abiotic flux measurements of two different NO-doped hydrogels (chitosan and alginate), and the NO diffusion coefficient in each of these hydrogels was determined based on Fick's first law of diffusion. We then demonstrate the versatility of the sensor by measuring NO transport in three model biological systems with known NO pathways, including thrombolites and stromatolites (bacterial communities), *Artemia salina* (animal), and *Arabidopsis thaliana* (plant) experiments. Results on concentration and flux measured with our NO microsensor correspond very well to the expected levels and trends for each one of these living systems, which validates the usability and versatility of this tool for physiology studies involving NO release.

Conflicts of interest

There are no conflicts to declare.

Acknowledgements

The authors thank the UF Agricultural and Biological Engineering Fellowship (PC), the Colombian funding agencies Colfuturo and Colciencias (DV; (No. 001375882), the USDA National Research Initiative (BAH; grant no. 2008-35100-19244), the UF Excellence Award (EMC; USDA/NIFA Hatch Project No. FLAABE-005062), NASA Exobiology and Evolutionary Biology Program (JSF; NNX12AD64G) and the NASA Florida Space Grant Consortium (EM and JF; grant no. 00091356) for funding.

References

1 T. S. Hakim, K. Sugimori, E. M. Camporesi and G. Anderson, *Physiol. Meas.*, 1996, **17**, 267–277.
2 X. Zhang, Y. Kislyak, J. Lin, A. Dickson, L. Cardosa, M. Broderick and H. Fein, in *Electrochemistry Communications*, 2002, vol. 4, pp. 11–16.
3 A. E. Christie, T. M. Fontanilla, V. Roncalli, M. C. Cieslak and P. H. Lenz, *Gen. Comp. Endocrinol.*, 2014, **195**, 28–39.
4 M. Jeseta, M. Marin, H. Tichovska, P. Melicharova, K. Cailliau-Maggio, A. Martoriati, A. Lescuyer-Rousseau, R. Beaujois, J. Petr, M. Sedmikova and J. F. Bodart, *PLoS One*, 2012, 7(7), e41509.
5 C. Nathan, *FASEB J.*, 1992, **6**, 3051–3064.
6 S. J. Neill, R. Desikan, A. Clarke, R. D. Hurst and J. T. Hancock, *J. Exp. Bot.*, 2002, **53**, 1237–1247.
7 D. Zeidler, U. Zä, I. Gerber, I. Dubery, T. Hartung, W. Bors, P. Hutzler, J. Rg Durner, U. Zahringer, I. Gerber, I. Dubery, T. Hartung, W. Bors, P. Hutzler and J. Durner, *Proc. Natl. Acad. Sci. U. S. A.*, 2004, **101**, 15811–15816.
8 F.-Q. Guo and N. M. Crawford, *Plant Cell*, 2005, **17**, 3436–3450.
9 E. Planchet and W. M. Kaiser, *Plant Signaling Behav.*, 2006, **1**(2), 46–51.
10 B. R. Crane, J. Sudhamsu and B. a. Patel, *Annu. Rev. Biochem.*, 2010, **79**, 445–470.
11 J. Sudhamsu and B. R. Crane, *Trends Microbiol.*, 2009, **17**, 212–218.
12 M. M. Tarpey and I. Fridovich, *Circ. Res.*, 2001, **89**, 224–236.
13 Z. H. Taha, *Talanta*, 2003, **61**, 3–10.
14 X. Ye, S. S. Rubakhin and J. V Sweedler, *Analyst*, 2008, **133**, 423–433.
15 I. R. Davies and X. J. Zhang, *Globins Other Nitric Oxide-Reactive Proteins, Pt A*, 2008, 436, pp. 63–95.
16 E. M. Hetrick and M. H. Schoenfisch, *Annu. Rev. Anal. Chem.*, 2009, **2**, 409–433.
17 B. J. Privett, J. H. Shin and M. H. Schoenfisch, *Anal. Chem.*, 2010, **82**, 4723–4741.
18 R. Trouillon, *Biol. Chem.*, 2013, **394**, 17–33.
19 J. Li, J. Xie, L. Gao and C. M. Li, *ACS Appl. Mater. Interfaces*, 2015, **7**, 2726–2734.
20 F. Bedioui, D. Quinton, S. Griveau and T. Nyokong, *Phys. Chem. Chem. Phys.*, 2010, **12**, 9976–9988.
21 Y. M. Liu, C. Punckt, M. A. Pope, A. Gelperin and I. A. Aksay, *ACS Appl. Mater. Interfaces*, 2013, **5**, 12624–12630.
22 Q. He, D. Zheng and S. Hu, *Microchim. Acta*, 2009, **164**, 459–464.
23 A. Merkoçi, *FEBS J.*, 2007, **274**, 310–316.
24 D. M. Porterfield, J. D. Laskin, S. K. Jung, R. P. Malchow, B. Billack, P. J. Smith and D. E. Heck, *Am. J. Physiol.: Lung Cell. Mol. Physiol.*, 2001, **281**, L904–L912.
25 E. S. Mclamore and D. M. Porterfield, *Chem. Soc. Rev.*, 2011, **40**, 5308–5320.
26 M. N. Friedemann, S. W. Robinson and G. a. Gerhardt, *Anal. Chem.*, 1996, **68**, 2621–2628.
27 J. J. Koehler, J. Zhao, S. S. Jedlicka, D. M. Porterfield and J. L. Rickus, *J. Phys. Chem. B*, 2008, **112**, 15086–15093.
28 P. Chaturvedi, D. C. Vanegas, M. Taguchi, S. L. Burrs, P. Sharma and E. S. McLamore, *Biosens. Bioelectron.*, 2014, **58**, 179–185.
29 J. P. Grotzinger and a. H. Knoll, *Annu. Rev. Earth Planet. Sci.*, 1999, **27**, 313–358.
30 D. C. Vanegas, G. Clark, A. E. Cannon, S. Roux, P. Chaturvedi and E. S. McLamore, *Biosens. Bioelectron.*, 2015, **74**, 37–44.
31 D. C. Vanegas, M. Taguchi, P. Chaturvedi, S. Burrs, M. Tan, H. Yamaguchi and E. S. McLamore, *Analyst*, 2014, **139**, 660–667.
32 M. Marvasi, I. A. Durie, E. S. Mclamore, D. C. Vanegas and P. Chaturvedi, *AMB Express*, 2015, **5**, 28–35.
33 E. S. McLamore, J. Shi, D. Jaroch, J. C. Claussen, a. Uchida, Y. Jiang, W. Zhang, S. S. Donkin, M. K. Banks,

K. K. Buhman, D. Teegarden, J. L. Rickus and D. M. Porterfield, *Biosens. Bioelectron.*, 2011, **26**, 2237–2245.
34 E. S. McLamore, D. M. Porterfield and M. K. Banks, *Biotechnol. Bioeng.*, 2009, **102**, 791–799.
35 H. Tajik, M. Moradi, S. M. R. Rohani, A. M. Erfani and F. S. S. Jalali, *Molecules*, 2008, **13**, 1263–1274.
36 Y. Zhang, C. K. Ng, Y. Cohen and B. Cao, *Mol. BioSyst.*, 2014, **10**, 1035–1042.
37 J. Luckanagul, L. A. Lee, Q. L. Nguyen, P. Sitasuwan, X. Yang, T. Shazly and Q. Wang, *Biomacromolecules*, 2012, **13**, 3949–3958.
38 S. L. Burrs, D. C. Vanegas, M. Bhargava, N. Mechulan, P. Hendershot, H. Yamaguchi, C. Gomes and E. S. McLamore, *Analyst*, DOI: 10.1039/c4an01788a.
39 I. G. Zacharia and W. M. Deen, *Ann. Biomed. Eng.*, 2005, **33**, 214–222.
40 C. Dupraz, R. P. Reid, O. Braissant, A. W. Decho, R. S. Norman and P. T. Visscher, *Earth-Sci. Rev.*, 2009, **96**, 141–162.
41 J. M. Mobberley, C. L. M. Khodadad and J. S. Foster, *Photosynth. Res.*, 2013, **118**, 125–140.
42 Y. L. Liu, Y. Zhao, Z. M. Dai, H. M. Chen and W. J. Yang, *J. Biol. Chem.*, 2009, **284**, 16931–16938.
43 G. Van Stappen, *FAO Fish. Tech. Pap.*, 1996, 295.
44 A. Heffer, J. W. Shultz and L. Pick, *Proc. Natl. Acad. Sci. U. S. A.*, 2010, **107**, 18040–18045.
45 J. S. Clegg, *J. Insect Physiol.*, 2011, **57**, 660–664.
46 S. Veeramani and V. Baskaralingam, *BioMetals*, 2011, **24**, 1035–1044.
47 M. C. Stensberg, R. Madangopal, G. Yale, Q. Wei, H. Ochoa-Acuña, A. Wei, E. S. McLamore, J. Rickus, D. M. Porterfield and M. S. Sepúlveda, *Nanotoxicology*, 2014, **8**, 833–842.
48 M. C. Stensberg, Q. Wei, E. S. McLamore, D. Porterfield, A. Wei and M. Sepulveda, *Nanomedicine*, 2011, **6**, 879–898.
49 K. Sun, K. Hunt and B. a. Hauser, *Plant Physiol.*, 2004, **135**, 2358–2367.
50 C. Xu and X. Qu, *NPG Asia Mater.*, 2014, **6**, e90.
51 D. Joung, V. Singh, S. Park, A. Schulte, S. Seal and S. I. Khondaker, *J. Phys. Chem. C*, 2011, **115**, 24494–24500.
52 N. A. Kotov, *Science*, 2010, **330**, 188–189.
53 Y. Lee, B. K. Oh and M. E. Meyerhoff, *Anal. Chem.*, 2004, **76**, 536–544.
54 H. H. Miao, J. S. Ye, S. L. Y. Wong, B. X. Wang, X. Y. Li and F. S. Sheu, *Bioelectrochem. Bioenerg.*, 2000, **51**, 163–173.
55 H. S. Jae, B. J. Privett, J. M. Kita, R. M. Wightman and M. H. Schoenfisch, *Anal. Chem.*, 2008, **80**, 6850–6859.
56 D. G. Wu, D. Cahen, P. Graf, R. Naaman, A. Nitzan and D. Shvarts, *Chem.–Eur. J.*, 2001, **7**, 1743–1749.
57 J. Katrlik and P. Zálešáková, in *Bioelectrochemistry*, 2002, vol. 56, pp. 73–76.
58 J. Hrbác, Č. Gregor, M. Machová, J. Králová, T. Bystroň, M. Číž and A. Lojek, *Bioelectrochemistry*, 2007, **71**, 46–53.
59 Y. Lee and J. Kim, *Anal. Chem.*, 2007, **79**, 7669–7675.
60 A. Dickson, J. Lin, J. Sun, M. Broderick, F. A. Harry and X. J. Zhang, *Electroanalysis*, 2004, **16**, 640–643.
61 K. A. Mowery and M. E. Meyerhoff, *Polymer*, 1999, **40**, 6203–6207.
62 M. Marvasi, A. S. George, M. C. Giurcanu, G. J. Hochmuth, J. T. Noel and M. Teplitski, *Food Microbiol.*, 2015, **46**, 139–144.
63 J. F. Stolz, R. P. Reid, P. T. Visscher, A. W. Decho, R. S. Norman, R. J. Aspden, E. M. Bowlin, J. Franks, J. S. Foster, D. M. Paterson, K. M. Przekop, G. J. C. Underwood and L. Prufert-Bebout, *Atoll Res. Bull.*, 2009, 1–31.
64 K. L. MYshrall, J. M. Mobberley, S. J. Green, P. T. Visscher, S. A. Havemann, R. P. Reid and J. S. Foster, *Geobiology*, 2010, **8**, 337–354.
65 A. Kumar, I. Castellano, F. P. Patti, A. Palumbo and M. C. Buia, *Nitric Oxide*, 2015, **47**, 34–39.
66 C. Y. Liu, D. J. Kieber, G. P. Yang, C. Xue, L. L. Wang and H. H. Liu, *Nitric Oxide*, 2014, **42**, 54–61.
67 M. Rao, B. C. Smith and M. A. Marletta, *mBio*, 2015, **6**, 1–10.
68 L. Plate and M. A. Marletta, *Trends Biochem. Sci.*, 2013, **38**, 566–575.
69 F. Chow, M. Pedersén and M. C. Oliveira, *J. Appl. Phycol.*, 2013, **25**, 1847–1853.
70 C. Dupraz and P. T. Visscher, *Trends Microbiol.*, 2005, **13**, 429–438.
71 F. Schreiber, P. Wunderlin, K. M. Udert and G. F. Wells, *Front. Microb. Immunol.*, 2012, **3**(372), 1–24.
72 J. M. Mobberley, C. L. M. Khodadad, P. T. Visscher, R. P. Reid, P. Hagan and J. S. Foster, *Sci. Rep.*, 2015, **5**, 12601.
73 J. Muñoz, A. Gómez, A. J. Green, J. Figuerola, F. Amat and C. Rico, *Mol. Ecol.*, 2008, **17**, 3160–3177.
74 T. H. MacRae, *Semin. Cell Dev. Biol.*, 2003, **14**, 251–258.
75 Y. Zhao, X. Ding, X. Ye, Z. M. Dai, J. S. Yang and W. J. Yang, *PLoS One*, 2012, **7**(2), e32129.
76 H. M. Robbins, G. Van Stappen, P. Sorgeloos, Y. Y. Sung, T. H. MacRae and P. Bossier, *J. Exp. Biol.*, 2010, **213**, 1464–1470.
77 M. Martin, M. J. R. Colman, D. F. Gómez-Casati, L. Lamattina and E. J. Zabaleta, *FEBS Lett.*, 2009, **583**, 542–548.
78 X. J. Zhu, J. Q. Dai, X. Tan, Y. Zhao and W. J. Yang, *BMC Dev. Biol.*, 2009, **9**, 1–8.
79 K.-H. Su, Y.-B. Yu, H.-H. Hou, J.-F. Zhao, Y. R. Kou, L.-C. Cheng, S.-K. Shyue and T.-S. Lee, *J. Cell. Physiol.*, 2012, **227**, 3053–3062.
80 E. Bess, B. Fisslthaler, T. Frömel and I. Fleming, *PLoS One*, 2011, **6**(6), e20848.
81 P. C. Bethke, F. Gubler, J. V. Jacobsen and R. L. Jones, *Planta*, 2004, **219**, 847–855.
82 K. Sun, Y. Cui and B. A. Hauser, *Planta*, 2005, **222**, 632–642.
83 S. Bhattacharjee, *Curr. Sci.*, 2005, **89**, 1113–1121.
84 M. Delledonne, Y. Xia, R. a. Dixon and C. Lamb, *Nature*, 1998, **394**, 585–588.
85 R. Ahlfors, M. Brosche, H. Kollist and J. Kangasjarvi, *Plant J.*, 2009, **58**, 1–12.

